ACS OMEGA

http://pubs.acs.org/journal/acsodf

Article

γ-Resistant Microporous CAU-1 MOF for Selective Remediation of Thorium

Nitin Gumber, Rajesh V. Pai,* Jitendra Bahadur, Somnath Sengupta, Debarati Das, and Uttam Kumar Goutam

Cite This: *ACS Omega* 2023, 8, 12268−12282

Read Online

ACCESS | Metrics & More | Article Recommendations | Supporting Information

ABSTRACT: A simple solvothermal method was used to synthesize a metal−organic framework (MOF) with an Al metal entity, viz., CAU-1 NH_2. The synthesized MOF was characterized using different techniques like X-ray diffraction, Fourier transform infrared spectroscopy, thermogravimetric analysis, scanning electron microscopy (SEM), field emission SEM (FE-SEM), transmission electron microscopy, small-angle X-ray scattering, positron annihilation lifetime spectroscopy, and X-ray photoelectron spectroscopy. The radiation stability was evaluated by irradiating the material up to a cumulative dose of 2 MGy using ^{60}Co for the first time. The studies showed a remarkable gamma irradiation stability of the material up to 1 MGy. The porosity and surface area of the synthesized MOF were determined by Brunauer−Emmett−Teller, which showed a high specific surface area of 550 m^2/g. The pH dependence study of Th uptake from an aqueous solution was performed from pH 2−8, followed by adsorption isotherm and adsorption kinetics studies. These results revealed that the Langmuir and pseudo-second-order kinetic models can be well adapted for understanding the Th uptake and kinetics, respectively. The synthesized MOF exhibited an ∼404 mg/g thorium adsorption capacity. Selectivity studies of adsorption of Th w.r.t. to U and different metal ions such as Cu, Co, Ni, and Fe showed that Th gets adsorbed preferentially as compared to other metal ions. In addition, the MOF could be used multiple times without much deterioration.

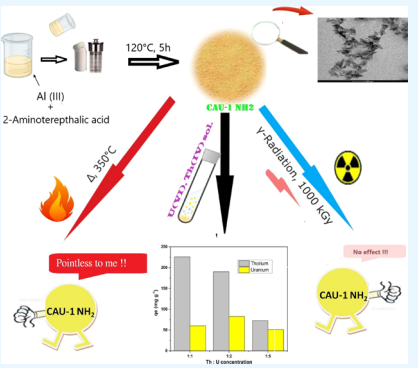

1. INTRODUCTION

The limited inventory of fossil fuels is expected to last for another 100 years. Apart from the inadequate reserve, it also possesses the risk of global warming due to the evolution of CO_2, and hence, a safe and secure source of energy is required to meet the needs to prevent global energy crisis.[1] A number of renewable energy sources like wind, solar, nuclear, and so forth could be used, but all of them have some limitations. Being a zero-emission source, nuclear energy is considered to be the future source of energy. Presently, uranium-based fuels are used all over the world. However, due to limited reserves of uranium, highly abundant thorium will become an alternate fuel material in place of uranium in the future nuclear reactors and may serve as a key fuel element and a valuable source to produce uranium as ^{233}U in breeder reactors. In principle, thorium is obtained from its mineral, monazite, through chemical separation.[2,3] Since the chemical and physical properties of uranium and rare-earth elements are comparable, selective separation of thorium becomes a bit strenuous when they co-exist. Conventionally, thorium is separated by liquid−liquid extraction by functional organic extractants such as tributyl phosphate, diphenyl phosphate, and so forth.[4,5] However, this process requires an enormous amount of organic extractants which become radioactive during the process, and disposal of such organic solvents poses threat to the environment. The presence of radioactive elements like U and Th in water streams leads to the accumulation in the liver of living organisms and hence poses serious health issues.[6] Adsorption-based methods possess a number of advantages over the conventional methods as they are simple and economic and have a high adsorption capacity.[7]

Because of the above reasons, development of a simple and efficient solid adsorbent which can be recycled effectively is highly desirable. Though a large class of solid adsorbents such as polymers,[8−12] membranes,[13,14] porous silica, mesoporous carbonaceous materials,[15−21] zeolites,[22] and porous nanomaterials[23] were explored in the past for the removal of Th(IV) from other metal ions, these adsorbents lack either selectivity or efficient reusability. Owing to the occurrence of large surface-to-volume ratio, high porosity, and availability of abundant sites for binding a specific metal ion, metal−organic frameworks (MOFs) are considered as next-generation adsorbents. These are three-dimensional coordination poly-

Received: December 30, 2022
Accepted: March 8, 2023
Published: March 23, 2023

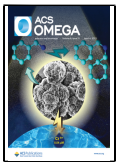

mers constituting an inorganic metallic node or a cluster and an organic linker giving rise to a framework with high porosity and suitable surface characteristics that are ideal for applications in diverse fields like catalysis, biomedical applications, magnetism, and water remediation.[24−27] Recently, a few MOFs[28−32] were exploited for selective sorption of Th(IV) and UO_2^{2+}, but the practical applicability of these frameworks is restricted due to limited adsorption capacity and low selectivity.

Sturdy and multipurpose MOFs have become urbane gallows to meet the genuine requirements of the nuclear community, but their features depend on the potency of their structure under the thermal, chemical, and mechanical environments and high radiation fields. Though many reports mention about the thermal, chemical, and mechanical stabilities of MOFs,[33] there is scarcity in the studies pertaining to the stability of MOFs under radiation.[34−36] According to previous reports, irradiation of MOFs induces many changes such as reduction in crystallinity, surface roughening, modification in surface area and pore characteristics, and so forth.[37,38] It has also been understood that the density and absorption cross section of the metal ion greatly influence the irradiation stability,[36] viz., a lower Z metal cation has a lower probability of absorbing the ionizing radiation. In this aspect, the MOF derived from Al^{3+} metal nodes such as CAU-1 NH_2 should be stable under gamma irradiation.

CAU-1 NH_2 (CAU stands for Christian-Albrechts-University, $[Al_4(OH)_2(OCH_3)_4(BDC\text{-}NH_2)_3]$) contains an aluminum metallic entity and 2-aminoterephthalic acid as the organic linker which is cost-effective due to high abundance of aluminum in the earth crust. Many MOFs reported in the literature like HKUST-1, DUT-4, and so forth are known to be water unstable and hence requires efforts to stabilize them in aqueous solutions.[39,40] In this regard, CAU-1 NH_2 with its strong structure possesses high aqueous and thermal stability and is thus designed for the adsorption of Th from different aqueous streams. Various synthetic methods commonly used are solvothermal, ultrasonication, mechanochemical, and electrochemical. In this study, we have employed the one-step solvothermal-based method for the synthesis of CAU-1 NH_2. The synthesized MOF was characterized using different techniques like X-ray diffraction (XRD), Fourier transform infrared spectroscopy (FT-IR), thermogravimetric analysis (TGA), Brunauer−Emmett−Teller (B.E.T.), scanning electron microscopy (SEM), SAX, transmission electron microscopy (TEM), positron annihilation lifetime spectroscopy (PALS), X-ray photoelectron spectroscopy (XPS), and so forth. Studies pertaining to Th adsorption were carried out by varying numerous experimental factors such as pH, concentration of Th, and equilibration time. Also, the selectivity studies among different metal ions including uranium and reusability of the MOF for successive adsorption were attempted. The presence of thorium in the reactors utilizing the Th−^{233}U cycle will invariably lead to the presence of intense γ-emitting isotopes like ^{208}Tl and ^{212}Bi (daughter products of ^{232}U). So, it is essential to estimate the gamma irradiation stability of the adsorbent. Thus, the gamma irradiation stability of CAU-1 NH_2 was evaluated for the first time up to 2000 kGy using ^{60}Co as the gamma source.

2. EXPERIMENTAL SECTION

2.1. Chemicals. We have used A.R. grade chemicals for the synthesis work without any further purification. Aluminum chloride ($AlCl_3{\cdot}6H_2O$) was purchased from SRL Pvt. Ltd., 2-aminoterephthalic acid was procured from Sigma-Aldrich, methanol from Anim Fine Chemicals (CH_3OH), and thorium nitrate ($Th(NO_3)_4{\cdot}5H_2O$) was obtained from Indian Rare Earth Ltd. We have used Milli-Q water for carrying out all dissolutions of the salts used in our experiments.

2.2. CAU-1 NH_2 Synthesis. CAU-1 NH_2 was synthesized using the procedure reported earlier using a high-pressure solvothermal method. In brief, 3 mmol of $AlCl_3{\cdot}6H_2O$ was taken in a beaker to which 14 mL of methanol was added. In another beaker, 1.75 mmol of 2-aminoterephthalic acid was added slowly to 14 mL of methanol. Both these solutions were mixed and stirred continuously for 1 h. The resulting solution was poured into an autoclave made up of stainless steel and heated to 125 °C for 5 h. It was then cooled to 25 °C. Further, it was centrifuged and washed twice with methanol. The obtained solid was then dispersed in water to remove the chloride ions from the pores if present. Finally a methanol wash was given for complete water removal, which was dried further at 100 °C under vacuum.

2.3. Characterization. XRD patterns were obtained on a Miniflex Rigaku-600 with a D/teX Ultra silicon strip detector using monochromatic Cu K_α (λ = 1.5406 Å) with 2θ from 6 to 60° at 2°/min scan rate. The FT-IR spectra were recorded on a Bruker make, tabletop model in the wavenumber ranging from 500 to 4000 cm^{-1}. To determine the typical size of the MOF nanoparticles, small-angle X-ray scattering (SAXS) measurement on the powder sample was carried out with a microfocus Cu K_α source. The two-dimensional (2D) SAXS data was collected using a multiwire gas detector. For morphology studies, SEM was carried out, whose details are provided in the Supporting Information (SI). The FE-SEM measurements of CAU-1 NH_2 powder samples were recorded prior and after Th adsorption by the GEMINISEM300 instrument [Make Carl Zeiss]. For this, the MOF powder was sprinkled on a sticky conducting carbon tape, and data was acquired at low voltage to avoid the charging effect. TEM images were recorded using the field emission-TEM model no. JEM-2100F. An acceleration voltage of 200 kV was used for TEM measurement with the sample dispersed in a carbon-coated 200 mesh Cu grid. PALS measurements were performed using a positron lifetime spectrometer comprising two fast-timing BaF_2 scintillation detectors with fast−fast coincidence circuitry. An ∼15 μCi of carrier-free ^{22}Na sandwiched between two 8 μm polyimide films (Kapton) was used as the positron source, which was implanted with sufficient quantity of the powder MOF sample to stop the positrons. In order to account for the amount of positron annihilating in the source itself, the lifetime spectrum of Si was used as a reference as per conventional practice. The lifetime spectra were acquired and further analyzed using PALSFit software.[41] The thermal stability of the as-synthesized CAU-1 NH_2 was investigated using Mettler Thermoanalyzer (model: TGA/SDTA851e/MT5/LF1600) by taking ∼100 mg of the sample in a thermobalance, which was heated to 873 K by flushing N_2 gas continuously with a heating ramp of 10 K min^{-1}. B.E.T. measurement was carried out for studying the adsorption−desorption characteristics on a SORPTOMATIC 1990 at liquid nitrogen temperature (77 K). Prior to the experiment, ∼100 mg of the sample was degassed at 10^{-2} mbar at 100 °C to remove any absorbed gas molecules or moisture. For radiation stability studies, the MOF was irradiated in a γ-irradiation facility (GC-5000) obtained from BRIT (Board of Radiation & Isotope Technology, Navi

https://doi.org/10.1021/acsomega.2c08274
ACS Omega 2023, 8, 12268−12282

Mumbai). The sample was positioned in a glass ampoule and irradiated using a 60Co γ-source. The gamma chamber used possess a dose rate of 4.7 kGy/h. The sample was irradiated for different durations such that cumulative doses of 200, 400, 600, 800, 1000, and 2000 kGy were imparted to the samples. After completion of each irradiation, the XRD and IR spectra were recorded for ascertaining the structural stability. XPS has been used for understanding the Th adsorption in CAU-1 NH_2. The experimental details are given in the Supporting Information.

2.4. Adsorption Studies. Before carrying out adsorption experiments, CAU-1 NH_2 was degassed under vacuum for 2 h. For carrying out Th adsorption studies, the thorium nitrate stock solution of concentration ∼2 M was prepared. The details of the solution preparation are given in the Supporting Information. Minute quantities of 0.1 M nitric acid and 0.1 M sodium hydroxide were used for pH adjustments. Batch method was used for the Th adsorption studies in the pH range 2−8. Approximately 5 mg of the sample was equilibrated with 20 mL of thorium nitrate solution for 5 h. The concentration of Th in the solution varied from 25 to 250 mg/L for adsorption isotherm studies. The kinetics was monitored by analyzing the Th concentration in the supernatant solution at different time intervals using total X-ray fluorescence (TXRF). The detailed instrumental description is provided in the Supporting Information. A typical TXRF spectrum fitted using PyMca software is shown as Figure S1. q_e, which is the adsorption capacity calculated using eq 1, is described below.

$$q_e = \frac{Ci - Cf}{m} \times V \quad (1)$$

2.5. Computational Studies. Density functional theory (DFT) calculations were applied to understand the geometric and electronic structure of the ligand and its corresponding thorium complex. The detailed information is given in the Supporting Information (SI).

3. RESULTS AND DISCUSSION

CAU-1 NH_2 consists of a tetragonal structure assembled by a pseudo bcc-type lattice with building blocks comprising 8-ring $[Al_8(OH)_4(OCH_3)_8]^{12+}$ units which are further joined through 12 aminoterephthalate ion linkers. This leads to the presence of an octahedral and tetrahedral cage having reachable diameters of 1 and 0.45 nm, respectively. The detailed cell structure and framework information can be obtained elsewhere.[42] Figure 1 shows the single unit cell of CAU-1 consisting of eight-ring units attached with aminoterephthalic acid (generated using CIF File 723320).

3.1. Characterization of MOFs. The XRD patterns of simulated CAU-1 and the synthesized compound are presented in Figure 2a. The compound crystallized into a tetragonal crystal structure as reported elsewhere with the *I*4/*mmm* space group.[42] The characteristic (011) reflection at 2θ = 6.9° and (022) reflection at 13.81° could be seen from Figure 2a. The reflection 2θ = 9.91° shows extra population of CAU-1 crystals at the −OH-terminated interface in the [002] direction. These two orientations of attachments of CAU-1 crystals are attributed to different reachable coordination locations of the inorganic structure. The broadening of peaks observed might be due to the nano nature of the MOF, which could also be seen in electron microscopy images.

Figure 2b shows the FT-IR spectrum of the synthesized CAU-1 NH_2. The asymmetric stretching of C═O at 1600 cm^{-1} and the symmetric stretching at 1430 cm^{-1} confirmed the binding of amino terephthalic acid with Al^{3+}. Further, the C−O stretching could be observed at ∼1070 cm^{-1}. The characteristic Al−O−Al stretching frequency at ∼605 cm^{-1} confirms the presence of Al−O−Al bonds in the MOF. The aliphatic C−H groups present in the methoxy part of the structure are ascertained through a band at ∼2900 cm^{-1}. The signature peaks of the primary amine were not clearly observed, which appear at the 3300−3450 cm^{-1} region that could be owing to the overlapping of O−H stretching at 3200−3500 cm^{-1}. The broad peak appeared suggests the presence of hydrogen bonding between N−H−O. However, the existence of a C−N bond could be established by the presence of a C−N aromatic stretching band at ∼1250 cm^{-1}. Thus, the aforementioned findings confirm the synthesis of CAU-1 NH_2.

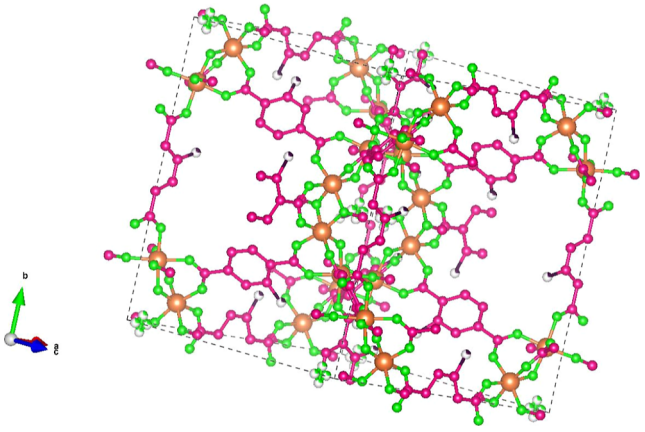

Figure 1. Single unit cell of CAU-1 NH_2 generated using the CIF file.

An aluminum-based MOF such as CAU-1 is known to be stable up to moderately high temperatures.[43] To assess the thermal stability of CAU-1 NH_2, the MOF powder sample was subjected to thermogravimetry. Figure 2c shows the % weight loss as the function of temperature. The TGA curve shows mainly three weight loss steps. The first step at ∼70−90 °C occurs due to the removal of water/methanol present. Further, the steady decrease observed up to ∼190 °C could be due to the removal of a small amount of entrapped H_2O molecules present inside the pores of the MOF. The elimination of the linkers starts beyond 200 °C and peaks at ∼350 °C. The last steep and continuous weight loss beyond 350 °C which accelerates further at around 490 °C is due to the complete removal of the carbonaceous framework, leaving only a stable Al_2O_3 phase.

3.2. Morphological and Particle Size Analysis. The morphological investigation of the MOF powder sample was studied by SEM, field emission SEM (FE-SEM), and TEM. The SEM images are shown as Figure S2. Figure 3a shows the FE-SEM image of the as-synthesized CAU-1 NH_2. It can be seen that CAU-1 NH_2 crystallized in the nano regime, which was confirmed further in TEM studies. Figure 3b−d shows the TEM images of CAU-1 NH_2 at different magnifications. These studies showed that the particle size ranges from 60 to 110 nm, and the particle size distribution calculated from TEM micrographs is provided in Figure S3. The TEM studies also revealed that the sample is highly porous in the order of 5−10 Å pores (Figure 3d). These pores are highly desirable for the sorption of Th(IV).

The particle size of CAU-1 NH_2 was also probed by SAXS. The 2D SAXS profile was radially averaged, and the scattering

https://doi.org/10.1021/acsomega.2c08274
ACS Omega 2023, 8, 12268−12282

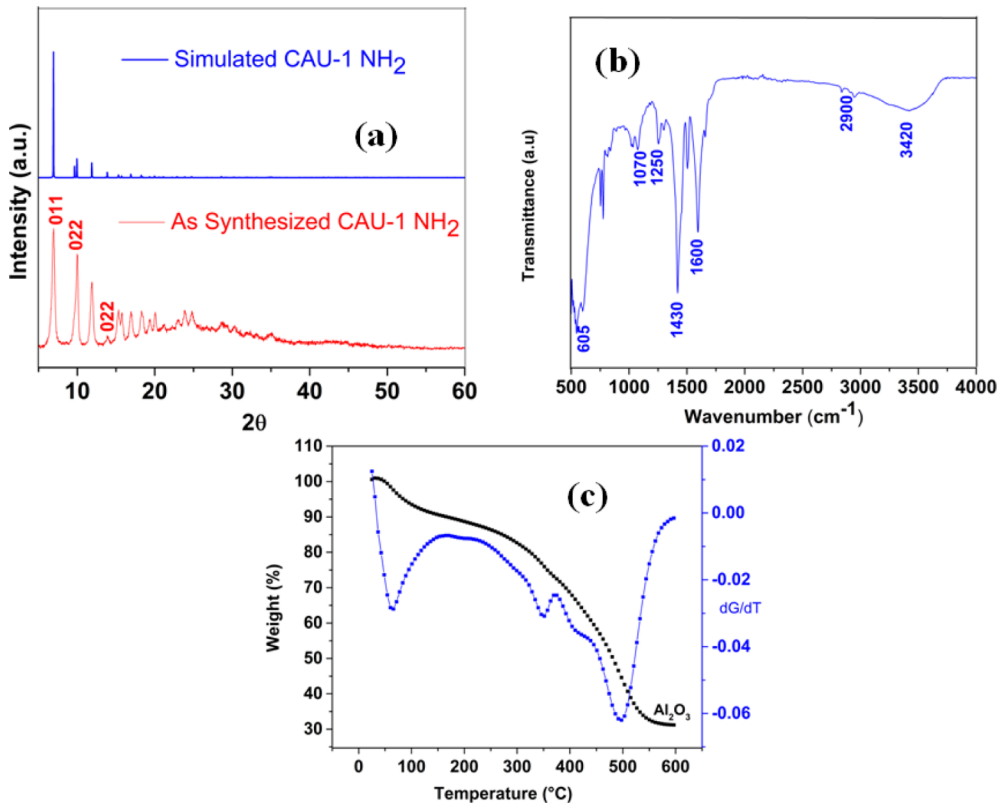

Figure 2. (a) XRD patterns of simulated and as-synthesized CAU-1 NH_2; (b) FT-IR spectrum of CAU-1 NH_2 and (c) TG curve of CAU-1 NH_2 powder sample.

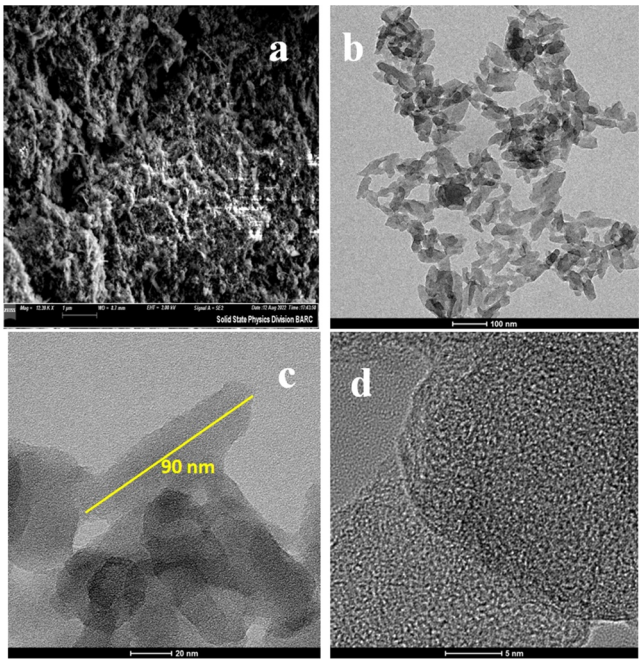

Figure 3. (a) FE-SEM micrograph and (b–d) TEM micrographs of CAU-1 NH_2 powder.

intensity is given as a function of wave vector transfer range Q which is defined as $4\pi \sin \theta/\lambda$ with 2θ being the scattering angle and λ being the wavelength of X-rays. The accessible Q-range was 0.1–2.5 nm^{-1}. The scattering intensity of the MOF sample is shown in Figure 4a. For simplicity, the scattering intensity of the MOF was modeled as an ensemble of polydisperse spheres (eq 2).

$$I(q) = N\Delta\rho^2 \int D(r)V(r)^2P(q, r)\mathrm{d}r \tag{2}$$

Here, $D(r)$ is the log-normal size distribution of MOF nanoparticles. The expression of the log–normal distribution (eq 3) can be written as

$$D(r, r_0, \sigma) = \frac{1}{\sqrt{2\pi^2\sigma^2r^2}} e^{\frac{-(\ln(\frac{r}{r_0}))^2}{2\sigma^2}} \tag{3}$$

Here, r_0 depicts the median radius and σ the polydispersity index. The average radius r_{av} can be written as $r_0e^{\sigma^2/2}$. $P(q,r)$ is the form factor of the sphere with radius r (eq 4).

$$P(q, r) = \left[\frac{3\{\sin(qr) - qr\cos(qr)\}}{(qr)^3}\right]^2 \tag{4}$$

The fitting of eq 2 is shown in Figure 4a, and the size distribution obtained using the above equation is shown in Figure 4b. The average size of the nanoparticle is ~70 nm, which is comparable to the typical size obtained from the TEM experiment.

3.3. Pore Size Measurements. Surface area, pore size, and its distribution are very important characteristics when we consider the adsorption of any metal ions from solution. A high value of specific surface area is desirable to have good adsorption characteristics. Moreover, the pore size and its distribution should be optimum to get utmost adsorption. The adsorption and desorption characteristics of CAU-1 NH_2 were determined by B.E.T. The adsorption–desorption isotherm of

https://doi.org/10.1021/acsomega.2c08274
ACS Omega 2023, 8, 12268–12282

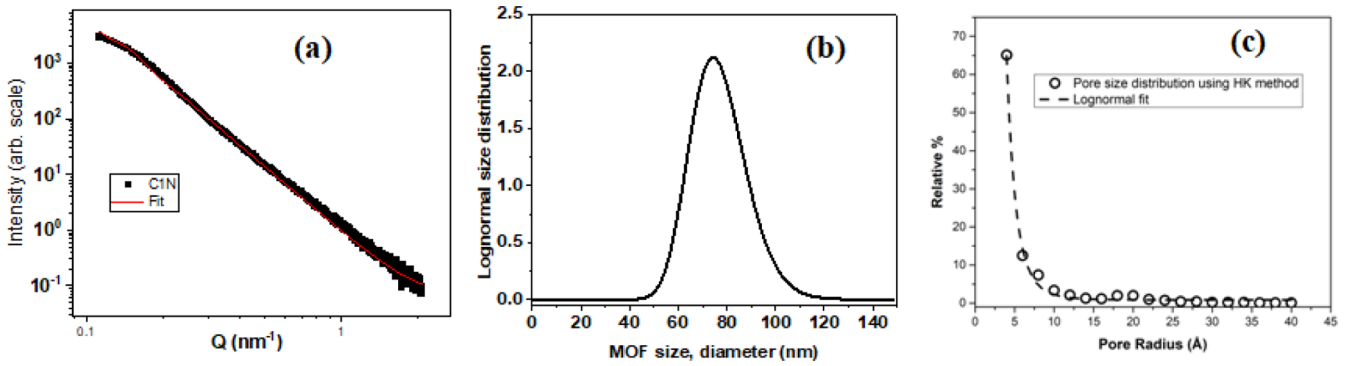

Figure 4. (a) SAXS profile of the CAU-1 NH_2 MOF sample. Solid line portrays the model fit to the data. (b) Estimated size distribution of the MOF nanoparticles and (c) pore size distribution of CAU-1 NH_2 using the N_2 adsorption−desorption isotherm fitted using log-normal distribution.

Table 1. Extracted Positron and *o*-Ps Pick-Off Annihilation Lifetime and Their Corresponding Intensities in CAU-1-NH_2

sample	τ_{1p} (ps)	τ_{2p} (ps)	T_{3p} (ns)	I_{1p} (%)	I_{2p} (%)	I_{3p} (%)
CAU-1 NH_2	205 ± 6	405 ± 6	2.340 ± 0.065	40.4 ± 2.5	57.8 ± 2.5	1.8 ± 0.7

the sample is shown as Figure S4. The sample possesses a high specific surface area of 550 $m^2\ g^{-1}$ with a pore volume of 0.32 $cm^3\ g^{-1}$. Figure 4c shows the pore size distribution of the as-synthesized MOF sample determined by the Horvath−Kawazoe (HK) method[44] and fitted using log-normal distribution.

These studies elucidated that the MOF exhibits mainly microporous structures with the pore radius ranging from 4 to 20 Å constituting micropores with the relative volume more than 90%. Pore size information of the MOF material was also probed by PALS. The lifetime spectra were acquired for approximately 1 million counts, and the experimentally acquired PALS spectrum of CAU-1 NH_2 was deconvoluted with the detector resolution function and further analyzed using PALSFit software. A typical PALS spectrum showing the different extracted lifetime components for CAU-1 NH_2 is presented as Figure S5. The extracted lifetime data are summarized in Table 1.

A positron interacts with a porous solid and annihilates either as a free and/or contained positron state or as a free and/or contained positronium (Ps) state.[45] Annihilation of positrons and Ps is more favored in the free volume holes which serve as localized sites compared to the bulk. Another annihilation mode, namely, pick-off annihilation, results by continuous collisions of contained Ps with the pore walls.

In the PALS study of CAU-1 NH_2, we observed three lifetime components. The first two lifetime components in the picosecond range are accredited to the positron annihilations in shallow traps and larger voids in the MOF material. The lifetime corresponding to the third component is in the range of typical pick-off annihilation and generally appears in *ortho* Ps (*o*-Ps). The corresponding pore size has been calculated using the Tau-Eldrup equation assuming spherical pores (eq 5).[46,47]

$$\frac{1}{\tau_{po}} = 2\left[1 - \frac{R}{R + \Delta R} + \frac{1}{2\pi}\sin\left(\frac{2\pi R}{R + \Delta R}\right)\right] \quad (5)$$

where τ_{po} (ns) and R (nm) are the *o*-Ps pick-off annihilation and the corresponding pore radius. The parameter $\Delta R = 0.166$ nm is an empirical value that represents an electron layer thickness on the pore surface. Using the above equation, the calculated pore size of CAU-1 NH_2 is $(d_{pore}) = 2R = 0.64 \pm 0.01$ nm. These results are in concurrence with the TEM and pore size distribution results by the HK method, establishing the microporosity of the MOF material. We have observed a low intensity of the pick-off annihilation. The resultant low intensity (I_{3p}) of this factor can be accredited to the existence of the Lewis acid center (Al^{3+}), which can suppress the *o*-Ps formation. A similar behavior was also observed by Warringham et al. in ZSM Zeolites, where both Bronsted and Lewis acidity decreased the amount of *o*-Ps detected.[48]

3.4. Gamma Radiation Stability Studies. For conventional metal ion adsorption, it is essential to study the chemical and aqueous stability of the material; however, for the radionuclide immobilization, radiation stability studies become a vital topic of interest since the presence of Th will invariably lead to the presence of a high γ-emitting radionuclide like ^{208}Tl and ^{212}Bi due to the attainment of radioactive equilibrium. Earlier reports have suggested Al-based MOFs to be highly resistant to γ-rays (refer the Introduction section); however, we did not come across any studies specific to the CAU-1-based MOF. Thus, to evaluate the γ-radiation stability of CAU-1 NH_2, it was irradiated with a very high dose of up to ∼2 MGy using ^{60}Co as the source. Post-irradiation studies were performed to check the effects on the structure of CAU-1 NH_2. No structural damage occurred up to 1 MGy, which could be established from the XRD studies. However, as the dose was increased to 2 MGy, altogether new XRD peaks were obtained, which did not match with the pristine MOF and thus resulted into decomposition of the framework. Figure 5 shows the XRD patterns of CAU-1 NH_2 prior and after irradiation. To assess the damage to atomic/functional groups, FT-IR spectra was also recorded and did not show any effect of irradiation up to 1 MGy. The corresponding FT-IR spectra are shown in Figure S6.

3.5. Adsorption Studies of Th. *3.5.1. Effect of pH.* pH is a principal constraint that significantly affects the nature and rate of adsorption of metal ions from an aqueous solution on the surface of MOFs. The speciation of metal in solution and the charge on the adsorbent resulting from protonation/deprotonation of specific sites are highly influenced by pH. It also affects the binding sites at the ligand surface. To assess the pH-dependent adsorption, the pH of the thorium-containing

https://doi.org/10.1021/acsomega.2c08274
ACS Omega 2023, 8, 12268−12282

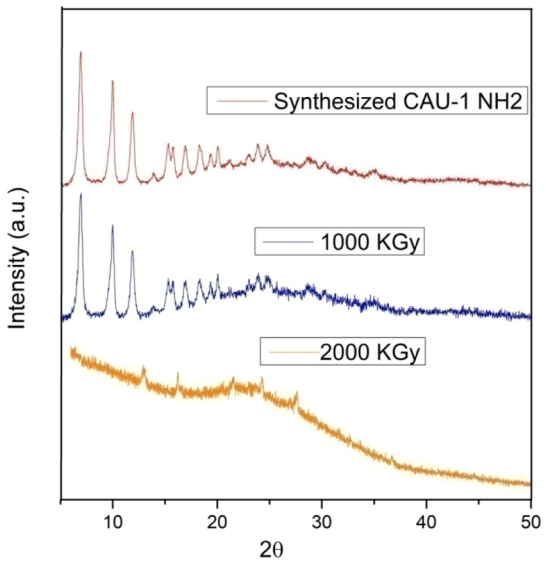

Figure 5. XRD pattern of the as-synthesized CAU-1 NH_2 before and after irradiation.

solution was varied from 2 to 8. The variation of Th(IV) adsorbed at different pHs is shown in Figure 6. The results

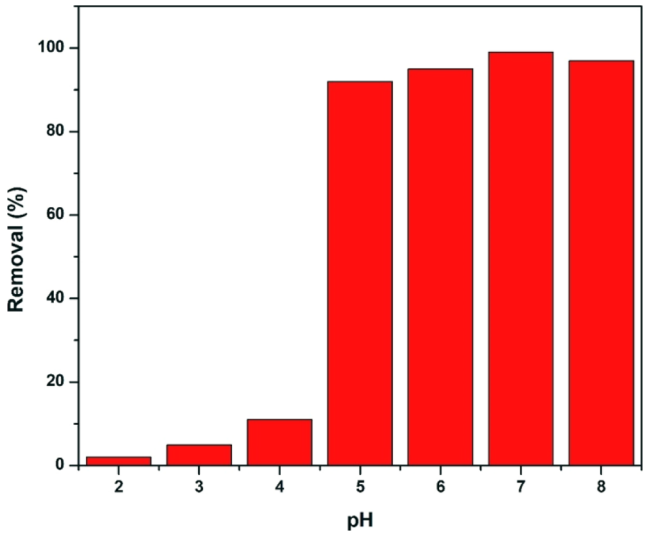

Figure 6. Removal of Th (IV) by adsorption on CAU-1 NH_2 at different pHs.

obtained showed a high dependency of pH for Th(IV) adsorption. At the lower pH region (2−4), the adsorption of Th is very less. However, beyond pH 4, almost 95% of Th (IV) got adsorbed, showing maxima at pH ∼7. Due to the occurrence of higher hydroxonium ions (H_3O^+), it may compete with Th^{4+}ions at lower pH, resulting in low adsorption capacity.[49] Also, hydroxonium ions would lead to the protonation of binding sites of the MOF, which includes $-NH_2$ and −OH groups, and result into a lower Th sorption. Instead, when the pH increases, the deprotonation may be taking place, resulting into the release of $-NH_2$ moiety in the MOF, and hence, more chance of chelation results in an increase in Th adsorption. Similar results have been reported widely in the literature.[50] The chemistry of Th is very complex in aqueous solutions, and still there is an ambiguity about exact species of Th at higher pH. The main species include Th^{4+}, $Th(OH)^{3+}$,$Th(OH)_2{}^{2+}$, $Th(OH)_3{}^{+}$, and finally $Th(OH)_4$,[10,51−53] and the key species at pH ∼ 5 is $Th(OH)_2{}^{2+}$. When the pH further increases (beyond pH = 7), $Th(OH)_4$ starts precipitating and hydrolyzing to form multinuclear complexes such as $[Th_2(OH)_2]^{6+}$, $[Th_4(OH)_8]^{8+}$, and $[Th_6(OH)_{15}]^{9+}$, which might have reduced the interaction with the MOF and hence a decrease in Th adsorption can be seen.[54] The type of these polymeric species will also be contingent on the strength of ions present in the medium. To avoid thorium precipitation as $Th(OH)_4$, our further experiments were centered at pH 5.

3.5.2. Adsorption Kinetics Studies. An ideal solid adsorbent should possess fast adsorption rate. The faster the kinetics, the lesser would be the energy required to attain equilibrium, and hence, the practicality of the material is more superior. The rate of adsorption of Th(IV) at MOF was studied by varying the time intervals (10−240 min). For this study, 100 mg/L Th(IV) (initial concentration) was taken. The adsorption kinetics was rapid during the initial time interval of 10−120 min, which was attributed to the free abundant active sites which was slowed down as the time progresses. Within 30 min of equilibration, ∼70% of the saturation level of adsorption was achieved. It was observed that the MOF attained equilibrium in 4 h, after which the adsorption capacity remained constant. The rate of adsorption of thorium with respect to time is presented in Figure 7c. According to the above observations, further experiments were conducted by fixing the equilibration time to 4 h. Adsorption kinetics was explored to extract the mechanistic information of sorption processes on the MOF by fitting the kinetic data using pseudo-first-order (PFO) as well as pseudo-second-order (PSO) model employing eqs 6 and 7, respectively.Here, q_t stands for adsorption capacity at time "t" (min), q_e = adsorption capacity at equilibrium, and k_1 and k_2 are rate constants of PFO and PSO, respectively.

$$\ln(q_t - q_e) = \ln q_e - k_1 t \tag{6}$$

$$\frac{t}{q_t} = \frac{1}{k_2 \cdot q_e{}^2} + \frac{t}{q_e} \tag{7}$$

Figure 7a,b represents the experimental data fitted with PSO and PFO kinetic models, respectively. The high correlation factor and comparable results between the calculated adsorption capacity and the experimental value suggested that this model (PSO) with $R^2 > 0.99$ is more relevant as compared to PFO with inferior $R^2 \sim 0.72$. The adaptation of PSO kinetics further confirms that the mode of sorption is mainly chemisorption rather than only physical adsorption on its surface. Thus, in the rate-controlling step, Th(IV) diffuses out and interacts with the MOF. Table 2 gives the kinetic data and rate constants obtained by using the two models.

3.5.3. Adsorption Isotherm Studies. The adsorption isotherm is a phenomenon that enlightens us about the interaction between the adsorbate molecule or ion with the surface sites available on the adsorbent molecule. Generally, this is carried out by analyzing the extent and nature of adsorption processes and correlating the equilibration data with a suitable empirical equation. To determine the maximum adsorption capacity of CAU-1 NH_2, adsorption isotherm studies were undertaken. Figure 8a represents the variation of adsorption capacity of CAU-1 NH_2 for Th(IV) at different initial concentrations. With the increase in the initial concentration of Th(IV), there observed an increase in

https://doi.org/10.1021/acsomega.2c08274
ACS Omega 2023, 8, 12268−12282

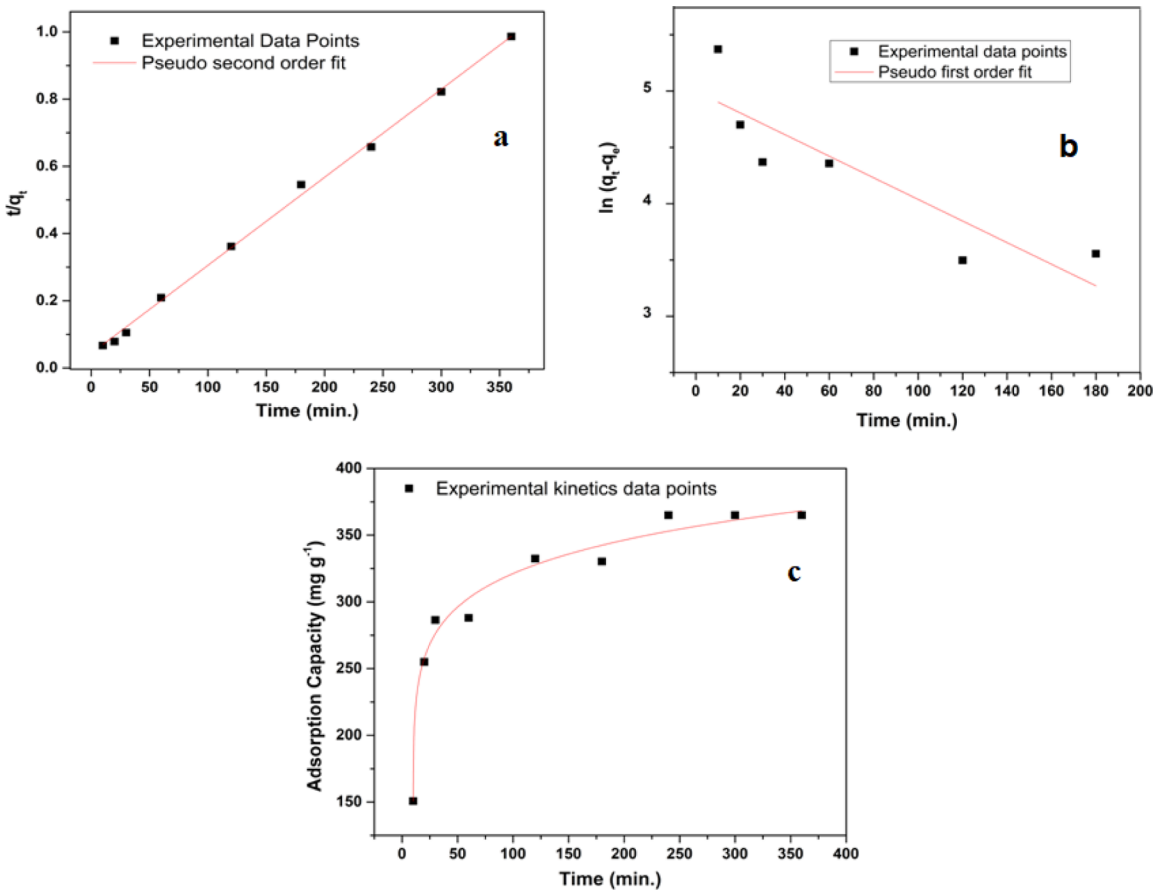

Figure 7. (a) Kinetic data fitted with the PSO model; (b) kinetic data fitted with the PFO model; and (c) effect of contact time of CAU-1 NH_2 with Th(IV) solution.

Table 2. Kinetic Data of Th(IV) Adsorption Obtained Using PFO and PSO Models

PFO model			PSO		
q_e (mg g^{-1})	k_1 (min^{-1})	R^2	q_e (mg g^{-1})	k_2 (g $mg^{-1}min^{-1}$)	R^2
142.6	0.0096	0.725	378.8	0.00018	0.998

adsorption capacity as many of the adsorption sites would still be vacant at lower Th concentration. The adsorption capacity reaches a constant value at higher concentration of Th. This implies that after a certain concentration, a plateau is formed (at the higher end of Figure 8a). This clearly shows that saturation of adsorption sites has reached. Models such as Langmuir, Freundlich, Temkin, and so forth elucidate the nature of adsorption isotherms and can explain most of the adsorption phenomena in solids. According to the Langmuir isotherm model, uniform and fixed adsorption sites are involved in the adsorption process as a monolayer.[55,56] In contrary to this, the Freundlich isotherm takes into consideration diversified energetics of adsorption at heterogeneous sites that result into multilayer formation.[57] Similarly, the Temkin isotherm deals with the heat of adsorption of molecules in the layer, which decreases with the increase of surface occupancy by adsorbate molecules.[58] We have used the above three mathematical models to comprehend the dispersal of adsorbate molecules on CAU-1 NH_2 and to extract the information of maximum adsorption capacity for Th(IV) ions.

The equations for Langmuir, Freundlich, and Temkin isotherms are given as eqs 8, 9, and 10 respectively.

$$\frac{C_e}{q_e} = \frac{1}{K_l \cdot q_{max}} + \frac{C_e}{q_{max}} \tag{8}$$

$$\text{Log } q_e = \text{Log } K_f + \frac{1}{n}\text{Log } C_e \tag{9}$$

$$q_e = B \ln C_e + B \ln K_T \tag{10}$$

In eq 8, q_e (mg g^{-1}) depicts the equilibrium adsorption capacity and q_{max} and K_l being the maximum adsorption capacity (mg g^{-1}) predicted by the Langmuir model and equilibrium binding constant, respectively (l mol^{-1}), in eq 9, Again q_e is the amount of ions sorbed at equilibrium (mg g^{-1}), C_e denotes the equilibrium concentration of the adsorbate (mg L^{-1}), whereas K_f and n are constants. In the Temkin mathematical expression (eq 10), B is the Temkin constant related to the heat of sorption and K_T is the Temkin equilibrium binding constant corresponding to the maximum binding energy calculated from adsorption isotherm studies. The experimentally obtained q_{max} was 404 mg/g, which is higher than most of the known adsorbents used till date for Th adsorption as shown in Table 3. This capacity can be reciprocated as 1.74 mmol g^{-1}, assuming the molecular formula of CAU-1 NH_2 as $Al_4(OH)_2(OCH_3)_4(BDC\text{-}NH_2)_3$). The detailed calculations are given in the Supporting Information.

https://doi.org/10.1021/acsomega.2c08274
ACS Omega 2023, 8, 12268−12282

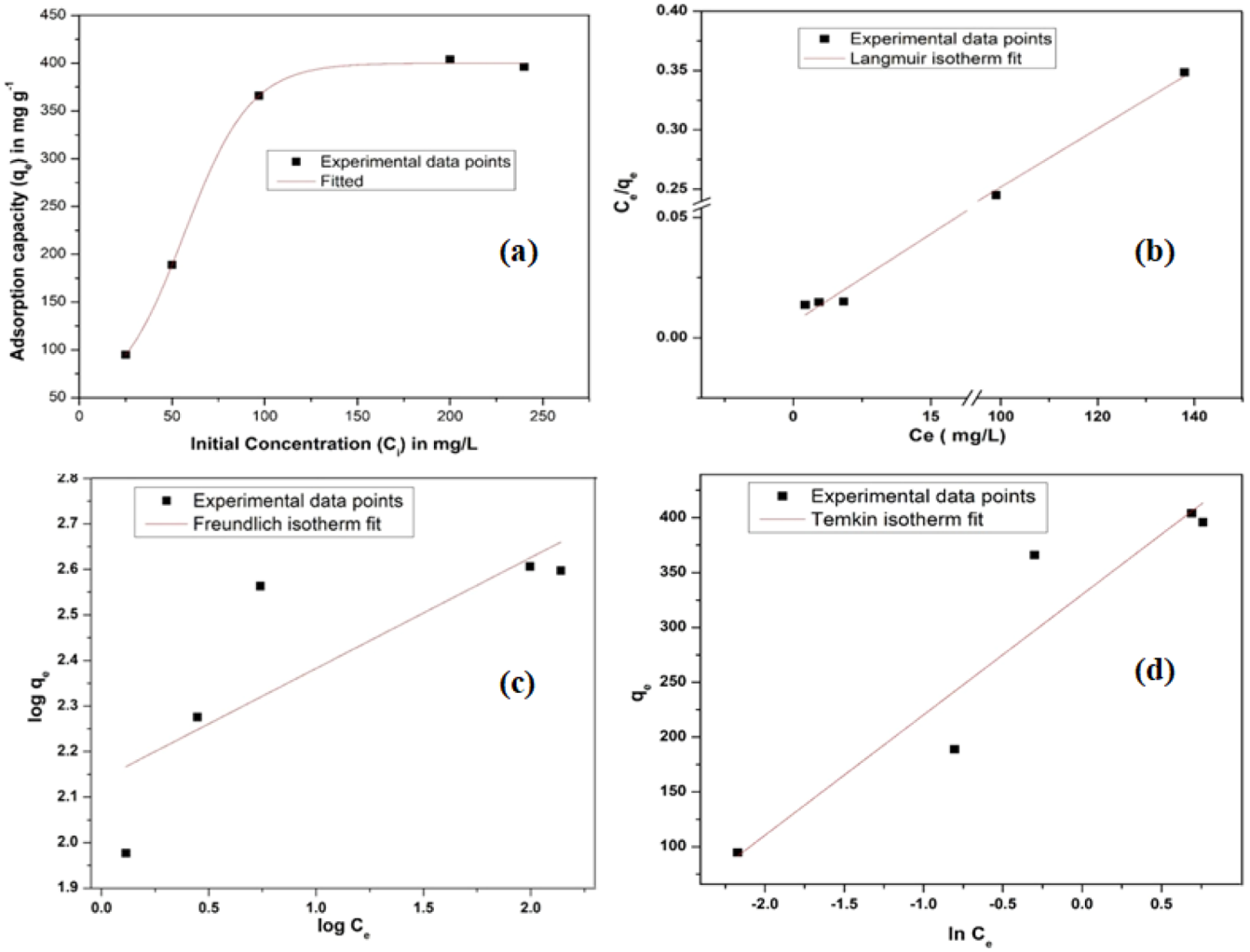

Figure 8. (a) Variation of adsorption capacity of CAU-1 NH_2 for Th(IV) at different initial concentrations; adsorption isotherms (b) assuming Langmuir model; (c) assuming Freundlich model; and (d) assuming Temkin model.

Table 3. Comparison of Adsorption Capacity of Th for Different Adsorbents

adsorbent	adsorption capacity (mg g^{-1})	references
MOF-LIC-SA	149	23
MIL-100(Al)	167	28
UiO-66-$(COOH)_2$	350	32
$Cu_3(BTC)_2$	757.08	59
UiO-66-OH	47.5	60
P_{15}	454	61
ANSC	252.5	62
amorphous SiO_2 (200−300 nm)	134.4	63
HQ-bentonite	65.44	64
CAU-1 NH_2	**404**	**this work**

Applying these above-mentioned isotherm models, it can be seen that the best fit was obtained for the Langmuir model, where R^2 = 0.999 and all others had a value inferior to this. Also, the close proximity of the calculated q_{max} using the Langmuir model and the experimentally observed value corroborate the above result. Thus, it can be inferred that the monolayer mechanism is dominant with chemisorption. Table 4 lists all the critical parameters of different isotherms. Figure 8b−d denote the Langmuir, Freundlich, and Temkin model isotherms for Th removal using CAU-1 NH_2.

3.5.4. Selectivity Studies. Th-based fuel after producing electricity through breeding followed by fission would contain a large number of other elements. Hence, it is essential to realize the interference of other metals on the adsorption behavior of Th(IV) for CAU-1 NH_2 MOF. Thus, to assess the selectivity of CAU-1 NH_2 for Th(IV) ions among other

Table 4. Adsorption Isotherm Parameters CAU-1 NH_2 Obtained Using Different Models

Langmuir model		Freundlich model		Temkin model	
parameter	value	parameter	value	parameter	value
q_{max}	406.5 mg g^{-1}	n	4.11	B	109.8 J mol^{-1}
K_l	0.39 L mol^{-1}	K_f	137.84 mg L^{-n} g^{-1} L^{n}	K_T	20.08 L g^{-1}
R^2	0.999	R^2	0.556	R^2	0.86

https://doi.org/10.1021/acsomega.2c08274
ACS Omega 2023, 8, 12268−12282

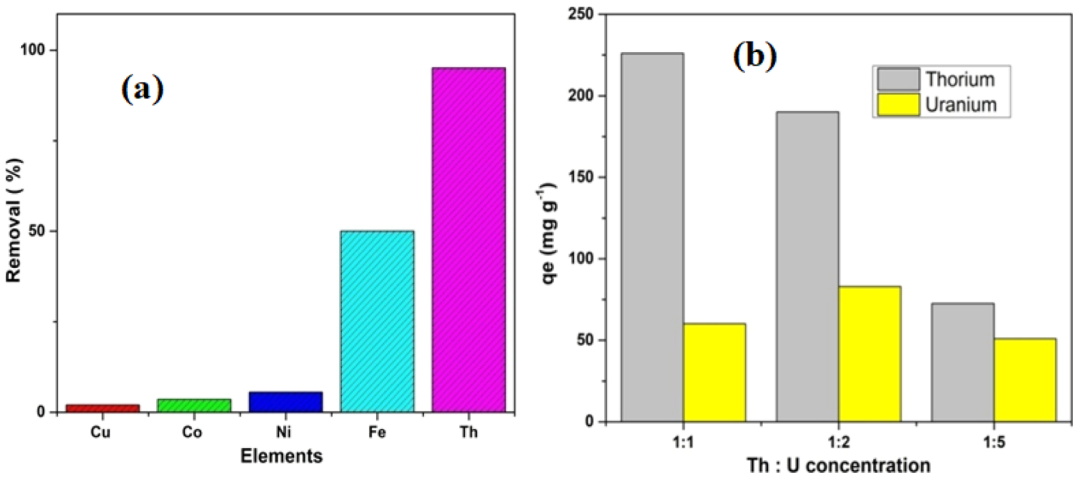

Figure 9. (a) Removal of different metal ions by adsorption on CAU-1 NH_2 MOF and (b) amount of Th and U co-adsorbed in CAU-1 NH_2 at different Th/U ratios.

competing metal ions, a stock solution was prepared containing Fe^{3+}, Co^{2+}, Ni^{2+}, Cu^{2+}, and Th^{4+} having similar concentrations of ∼20 mg/L. The studies showed that Th could be adsorbed on the MOF almost quantitatively (>95%) in the presence of these ions. Among them, Fe was the most interfering ion with an adsorption of ∼50%, and none of the others had any much affinity to the MOF synthesized and hence showed the least interference. Transition metal ions in their lower oxidation state such as Fe^{2+}, Co^{2+}, Ni^{2+}, Cu^{2+}, and so forth are moderately softer acids due to their lesser charge density (lower ionic charge/ionic size ratio) when compared to Fe^{3+}, which has got comparatively higher charge density. Similarly, Th^{4+} is a hard acid, which binds with ease with any hard base such as the $-NH_2$, $-OH$ group present in the MOF according to the HSAB theory.[65] Because of these reasons, the binding and % removal by adsorption are exclusively higher for Th^{4+} compared to those for other metal ions. In addition to the adsorption of different metal ions, the adsorption characteristics of the counter NO_3^- ion were also investigated at pH 5. As the concentration was less, the amount of NO_3^- ion adsorbed on the MOF was insignificant. These details are given in the Supporting Information and in Table S1.

3.5.4.1. Selectivity between U and Th. Since uranium is always produced in the reactor where Th is utilized as a fuel material, it is important to know the selectivity for Th against different proportions of U present in the aqueous solution for practical applicability in considering the selectivity of MOF. Thus, studies were performed keeping in mind the different ratios of U and Th to mention 1:1, 1:2, and 1:5.

In all the ratios studied, it was observed that the selectivity of thorium was much better in comparison to that of uranium. The preferential adsorption toward thorium is attributed to the higher ionic potential of Th^{4+} ions (charge/size). In the case of actinide elements, the complexation tendency decreases in the order $M^{4+} > MO_2^{2+} > M^{3+}$ due ionic potential. Due to the association of oxygen atoms in the uranyl entity, the average charge on uranium is around 3.3.[66] Even though the adsorption capacity of Th was seen to be decreasing with an increase in the ratio of U/Th, Th was preferred over U for all the cases studied. The decrease of Th adsorption with an increase in U/Th is due to the higher competition of UO_2^{2+}over Th^{4+} due to its high abundance. Figure 9a shows the ease of removal of various metal ions studied, and Figure 9b shows the amount of Th and U adsorbed simultaneously at different Th/U ratios.

3.5.5. Reusability Studies. After adsorption, it is important to consider the reusability of the MOF by successive adsorption−desorption cycles. Thus, a number of eluting media like HNO_3, HCl, Na_2CO_3, and NaOH at different concentrations were employed to desorb Th(IV) ions from the MOF. It was observed that the CAU-1 NH_2 synthesized was neither stable in highly acidic conditions nor in high basic conditions (0.1−0.3 M). Both these media caused disintegration of the MOF and yielded colored solutions. Thus, acids such as HNO_3 and HCl (moderate acidity of 0.01 M) were used for elution of Th adsorbed from the MOF. Even though the MOF decomposed in 0.01 M HCl during the third cycle, it was quite stable in 0.01 HNO_3 and hence subsequently chosen as the eluting medium. Figure 10 shows the relative percentage of Th adsorbed during each successive cycle. As observed from the figure, the tendency of Th adsorption decreases as the numbers of cycles increased, and this could be due to the combination of fractional loss of MOF during removal of supernatant after centrifugation and partly ineffective stripping of Th using a 0.01 M HNO_3 solution. Nevertheless, Th could

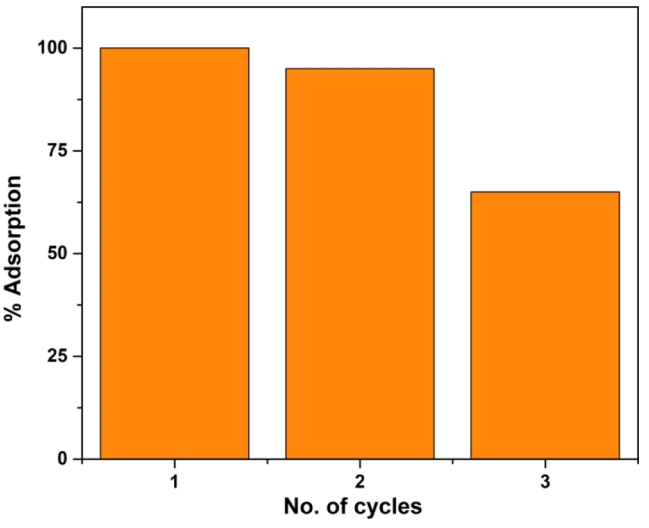

Figure 10. % of Th adsorbed in CAU-1 NH_2 in successive cycles.

https://doi.org/10.1021/acsomega.2c08274
ACS Omega 2023, 8, 12268−12282

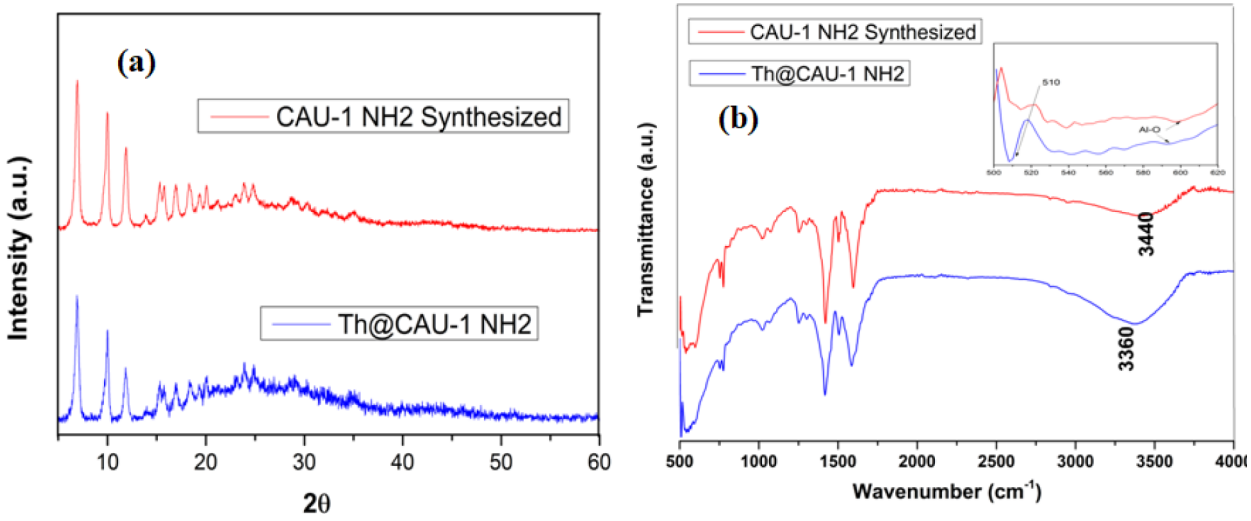

Figure 11. (a) XRD pattern of CAU-1 NH_2 prior and after Th adsorption and (b) FT-IR spectra of CAU-1 NH_2 prior and after Th adsorption.

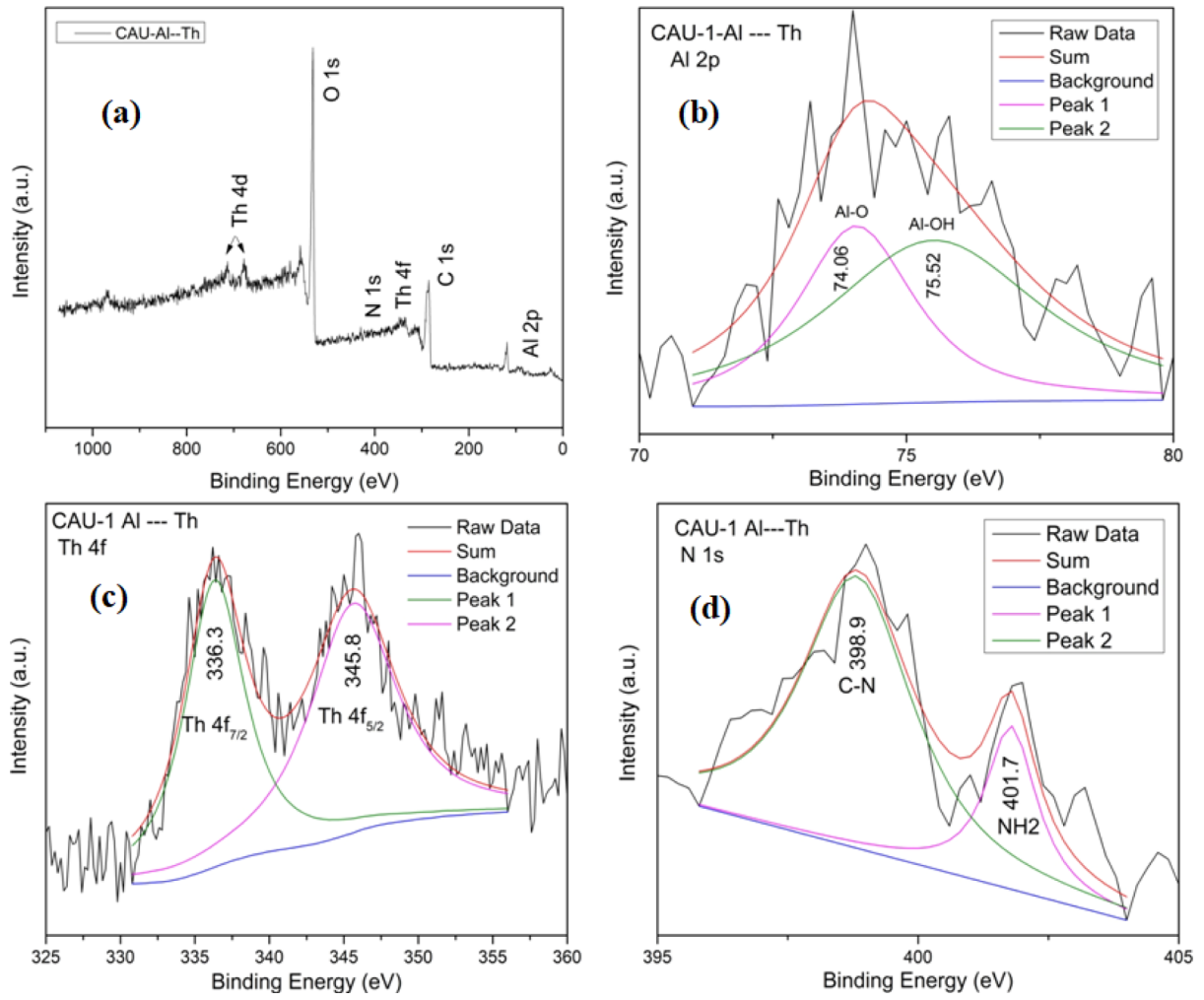

Figure 12. XPS spectra of CAU-1 NH_2 after Th adsorption: (a) survey scan; (b) Al 2p; (c) Th 4f; and (d) N 1s.

be adsorbed ~65% even for the third cycle, and hence, MOF could be utilized for successive cycles. In future, efforts would be put up to improve the recyclability studies.

3.5.6. Probable Adsorption Mechanism. It is very important to know the mode of adsorption of metal ions. In order to ratify the mechanism of adsorption involved, we have carried out XRD, FT-IR, and XPS after Th adsorption and compared with the sample prior to adsorption. Also, computational-based models were used to understand the adsorption mechanism. First, XRD studies revealed that there was no change in the structure of MOF before and after adsorption of Th as can be seen from Figure 11a. This

https://doi.org/10.1021/acsomega.2c08274
ACS Omega 2023, 8, 12268−12282

confirms that the Al metal cluster does not get affected by Th adsorption. In post-IR experiments, we observed some changes when compared to sample prior to Th adsorption. As described earlier, comprehensible NH_2 peaks were not observed due to the occurrence of hydroxyl groups (γO−H).[67] However, a red shift in the region 3200−3400 cm^{-1} is observed, which explains the role of NH_2 and O−H groups participating in the chelation of Th as shown in Figure 11b. In addition to this, a shift in the Al−O stretching frequency was also observed, which could be due to the participation of (−OH) bonds for adsorption and is supported further by XPS experiments. An additional peak due to the formation of O/N−Th bond at around 510 cm^{-1} could be seen in the Th-adsorbed sample. This peak was absent in the case of bare MOF, which can be seen from the inset of Figure 11b. Similar results were obtained by Kazy et al.[68] in their uranium and thorium sequestration studies on biomass at 800−400 cm^{-1}, which was assigned to the formation of δ (M−O) and δ (O−M−O) bonds (M = metal ion). The rest of the spectrum was almost identical to the MOF prior to Th adsorption. This confirms that adsorption of Th occurs through $-NH_2$ and −OH associated with Al via the chelating mechanism.

Further, XPS studies were carried to get a comprehensive insight of the adsorption mechanism. Figure 12 shows the XPS recorded after Th adsorption. The survey scan depicted in Figure 12a clearly shows the presence of characteristic 4f and 4d peaks of Th apart from the main four elements Al, N, C, and O which are marked at the respective positions. The XPS spectrum (full range) and the deconvoluted scans of individual elements of bare CAU-1 NH_2 (prior to Th adsorption) are shown in Figure S7. As the intensity of C and O peaks was so high that these were overshadowing the presence of N, a magnified image with deconvoluted peaks is shown in the inset of Figure S7a. Two peaks at 398.7 and 400.3 eV were obtained, which could be assigned to the N (1s) peaks of C−N and NH_2 groups, respectively, which are shifted to 398.9 and 401.7 eV, respectively post-adsorption and confirms the participation of NH_2 groups.[69] We also observed a slight blue shift of Al (2p) peaks in the samples containing Th, which hinted in the involvement of O attached to Al in the adsorption of Th ions. Due to this interaction, the electron density of the Al metal reduced, resulting into an increase in the binding energy of Al (2p) after Th adsorption. The Al (2p) peaks before and after Th adsorption are shown in Figures S7b and 12b, respectively. Figure 12c shows the deconvoluted Th $f_{7/2}$ and Th $f_{5/2}$ appearing at 336. 3 and 345.8 eV, respectively. These Th (4f) peaks were in agreement with the values reported in the literature, confirming the presence of Th(IV) ions.[70] Further, the role of O could also be confirmed by observing a slight shift in the C (1s) XPS spectra after Th adsorption as shown in Figure S7c,d. The role of amino/−OH groups can be pictorially represented as eq 11. The mechanism was further supported by structure modeling and DFT-based computation studies.

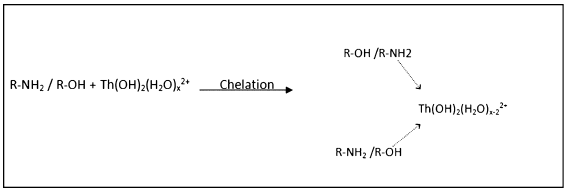

(11)

In the computational work, aniline was used as a simplified molecule to model the binding site of the MOF during the DFT calculation. Modeling the entire MOF is computationally difficult due to which this simplified moiety was used to elucidate the interaction behavior of the MOF with Th(IV). The ligand, aniline, was subjected to geometry optimization at the RI-BP86-D3BJ/def2-TZVP level to obtain its lowest energy structure.

According to the literature, the Th(IV) ion exists mainly as $Th(OH)_2(H_2O)_7^{2+}$ around pH 5, where the adsorption studies are performed.[71] Since the primary coordination sphere of Th(IV) in an aqueous solution is composed of nine molecules, various starting geometries of the $Th(OH)_2(H_2O)_6$−aniline complex were obtained by replacing the water molecule and keeping the number of donor atoms directly bonded to thorium to be 9.[72] In a similar manner, systematic geometry optimization was performed to obtain the lowest energy structure for the $Th(OH)_2(H_2O)_6$−aniline complex. The corresponding lowest energy structures for $Th(OH)_2(H_2O)_7^{2+}$, aniline, and $Th(OH)_2(H_2O)_6$−aniline complex are shown in Figures 13a−c. Also, harmonic vibrational frequency analysis was done to characterize the lowest energy structure as energy minima in the potential energy surface.

In order to elucidate the metal−ligand interaction in the thorium−aniline complex, natural bond orbital analysis was performed. The positive charge on the acceptor atom of Th decreased from 1.74 in the $Th(OH)_2(H_2O)_7^{2+}$ complex to 1.70 in the $Th(OH)_2(H_2O)_6$−aniline complex, suggesting an electronic charge transfer from ligand to metal during the complexation process. Also, the Wiberg bond index, which can be used to quantify the strength of the Th−N (aniline) bond in the complex, shows a value of 0.29. This indicates that a moderate interaction exists between the acceptor and donor atoms.

An "atoms in molecules" analysis was also carried out to get understanding of the nature of bonding operating between thorium ligand in the complex. The properties of the Th−N bond critical points (bcp's) such as electron density (ρ_b), the Laplacian of electron density ($\nabla^2\rho_b$), and the energy density at the bcp (H_b) are listed in Table 5. The calculated ρ_b value was found to be 0.034 $e^-/bohr^3$ at the Th−[N](ligand) critical point, which is comparatively similar to the electron density calculated for the LiF molecule, indicating that the metal−aniline bond is possessing an ionic character.[73] The positive value of the Laplacian of electron density indicates a closed-shell interaction in the complexes, indicating that the metal−ligand bond is indeed ionic.

In order to estimate the complexing ability of the ligand with the thorium ion, we have calculated the complexation energy for the metal complex using eq 12, from the energy difference between products and reactants.

$$Th(OH)_2(H_2O)_7^{2+} + \text{aniline} \rightarrow Th(OH)_2(H_2O)_6 - \text{aniline}^{2+} + H_2O \quad (12)$$

The estimated complexation energies at the RI-BP86-D3BJ-ZORA-def2-TZVP (gas phase) level shows a value of −15.17 kcal/mol, indicating the feasibility of the metal−ligand binding process.

4. CONCLUSIONS

A highly γ-resistant (up to 1 MGy) CAU-1 NH_2 MOF was synthesized using a simple one-pot solvothermal method. The

https://doi.org/10.1021/acsomega.2c08274
ACS Omega 2023, 8, 12268−12282

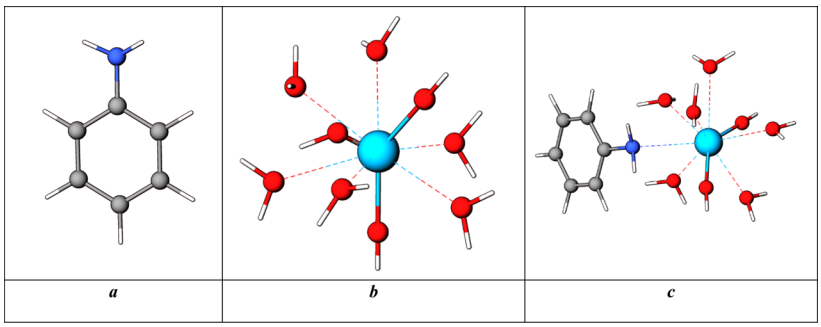

Figure 13. Optimized geometries of the lowest energy structure for (a) aniline, (b) $Th(OH)_2(H_2O)_7^{2+}$, and (c) $Th(OH)_2(H_2O)_6$-aniline^{2+} at the BP86/def2-TZVP level. Color code: gray balls represent carbon, blue balls represent nitrogen, red balls represent oxygen, light big blue ball represents thorium, and white color represents hydrogen atoms.

Table 5. Properties of bcps for the M−[N](Ligand) Bond in the $Th(OH)_2(H_2O)_6$−aniline^{2+} Complex

molecule	Th−[N] (ligand)		
thorium−aniline complex	ρ_b	$\nabla^2\rho_b$	H_b
	+0.03	+0.07	−0.003

synthesized MOF exhibited good thermal stability up to 350 °C. The N_2 adsorption−desorption isotherm yielded a high surface area and a large pore volume. The morphological studies by TEM and SAXS showed that the material synthesized was nano in nature. The pore size calculated using B.E.T. and PALS unveiled it to be microporous in nature. Though the synthesized MOF was stable in moderately acidic and basic conditions, it was not stable at high acidic and basic conditions. Based on the speciation of Th(IV) ions at different pH conditions, it was observed that pH = 5 was ideal for good thorium adsorption characteristics. The prompt adsorption kinetics during the initial adsorption cycle was attributed to the abundant active sites, which slowed down as the time progresses. The MOF showed a high adsorption capacity of ∼404 mg/g for Th, and its preferential adsorption compared to many metal ions including UO_2^{2+} ascertained that it is highly suitable for Th(IV) separation from aqueous streams. The high correlation factor obtained for PSO kinetics and its corroboration with the experimental results showed that the mode of sorption is mainly chemisorption rather than mere physical adsorption on its surface. The reusability studies postulated encouraging results, which showed that Th could adsorb ∼65% even for the third cycle and hence demonstrated the usability of CAU-1 NH_2 MOF for successive adsorption cycles. The adsorption mechanism studied by FT-IR and XPS after Th adsorption confirms that the adsorption of Th occurs through $-NH_2$/−OH functional groups via the chelation mechanism. Moderately high complexation energy of the Th−N ligand center implied high feasibility of the metal−ligand binding process studied by the DFT-based computational method. Thus, these studies provide a solid proof that inexpensive MOF like CAU-1 could be used for radionuclide's sequestration from aqueous solutions.

■ ASSOCIATED CONTENT

Supporting Information

The Supporting Information is available free of charge at https://pubs.acs.org/doi/10.1021/acsomega.2c08274.

Experimental details for SEM analysis; Th stock solution preparation; TRXF measurements; calculation of adsorption capacity in molar basis; nitrate estimation using titrimetry; computational analysis; TXRF spectra fitted using PyMca software; SEM images of the as-synthesized CAU-1 NH_2; particle size distribution of CAU-1 NH_2 calculated from TEM images; N_2 adsorption−desorption isotherm using B.E.T.; PALS spectrum of CAU-1 NH_2 showing different extracted lifetime components; FT-IR spectrum before and after 200, 400, 600, 800, and 1000 kGy γ-dose; XPS spectra of CAU-1 NH_2 prior to Th adsorption; % removal of metal ions and counter NO_3^- ion on MOF carried out at pH 5; and references (PDF)

■ AUTHOR INFORMATION

Corresponding Author

Rajesh V. Pai − *Fuel Chemistry Division, Bhabha Atomic Research Centre, Mumbai 400085, India; Homi Bhabha National Institute, Anushaktinagar, Mumbai 400094, India;* orcid.org/0000-0002-9258-2751; Email: rajeshvp@barc.gov.in

Authors

Nitin Gumber − *Fuel Chemistry Division, Bhabha Atomic Research Centre, Mumbai 400085, India; Homi Bhabha National Institute, Anushaktinagar, Mumbai 400094, India*

Jitendra Bahadur − *Solid State Physics Division, Bhabha Atomic Research Centre, Mumbai 400085, India; Homi Bhabha National Institute, Anushaktinagar, Mumbai 400094, India;* orcid.org/0000-0002-2547-2907

Somnath Sengupta − *Material Chemistry and Metal Fuel Cycle Group, Indira Gandhi Centre for Atomic Research, Kalpakkam, Tamil Nadu 603102, India*

Debarati Das − *Radiochemistry Division, Bhabha Atomic Research Centre, Mumbai 400085, India; Homi Bhabha National Institute, Anushaktinagar, Mumbai 400094, India*

Uttam Kumar Goutam − *Technical Physics Division, Bhabha Atomic Research Centre, Mumbai 400085, India*

Complete contact information is available at: https://pubs.acs.org/10.1021/acsomega.2c08274

Author Contributions

The manuscript was written through contributions of all authors. All authors have given approval to the final version of the manuscript.

Notes

The authors declare no competing financial interest.

https://doi.org/10.1021/acsomega.2c08274
ACS Omega 2023, 8, 12268−12282

■ ACKNOWLEDGMENTS

The authors would like to thank Dr. S. Kannan, Director, RC & IG, for his immense support in favor of the work. The authors also acknowledge Dr. S Chaudhury, Head, Fuel Chemistry Division, for his constant back-up. The authors thank Dr. Ruma Gupta and Smt. Geeta Patkare for carrying out SEM and TGA analysis, respectively. The authors appreciate Dr. A.K. Dubey for helping in carrying out irradiation experiments. The authors are also grateful to Smt. Pallavi Mohare and Vishakha Sarode for helping in adsorption experiments. The authors acknowledge DST & SAIF/CRNTS, IIT Bombay, for carrying out TEM measurements. The authors are grateful to Dr. Jagannath and Dr. Kaushik Sanyal for helping in XPS and TXRF experiments, respectively.

■ REFERENCES

(1) Solomon, S.; Plattner, G.-K.; Knutti, R.; Friedlingstein, P. Irreversible climate change due to carbon dioxide emissions. *Proc. Natl. Acad. Sci. U.S.A.* **2009**, *106*, 1704−1709.
(2) Vaggelli, G.; Borghi, A.; Cossio, R.; Fedi, M.; Giuntini, L.; Lombardo, B.; Marino, A.; Massi, M.; Olmi, F.; Petrelli, M. Micro-PIXE Analysis of Monazite from the Dora Maira Massif, Western Italian Alps. *Microchim. Acta* **2006**, *155*, 305−311.
(3) Maes, S.; Zhuang, W.-Q.; Rabaey, K.; Alvarez-Cohen, L.; Hennebel, T. Concomitant Leaching and Electrochemical Extraction of Rare Earth Elements from Monazite. *Environ. Sci. Technol.* **2017**, *51*, 1654−1661.
(4) Nasab, M. E.; Sam, A.; Milani, S. A. Determination of optimum process conditions for the separation of thorium and rare earth elements by solvent extraction. *Hydrometallurgy* **2011**, *106*, 141−147.
(5) Dong, Y.; Li, S.; Su, X.; Wang, Y.; Shen, Y.; Sun, X. Separation of thorium from rare earths with high-performance diphenyl phosphate extractant. *Hydrometallurgy* **2017**, *171*, 387−393.
(6) Vicente-Vicente, L.; Quiros, Y.; Pérez-Barriocanal, F.; López-Novoa, J. M.; López-Hernández, F. J.; Morales, A. I. Nephrotoxicity of Uranium: Pathophysiological, Diagnostic and Therapeutic Perspectives. *Toxicol. Sci.* **2010**, *118*, 324−347.
(7) Malekynejad, A.; Sepehrian, H.; Manoochehri, M. Adsorption of Thorium from Aqueous Solution using Nanoporous Adsorbents: Effect of Contact Time, pH, Initial Concentration, and Temperature. *Part. Sci. Technol.* **2013**, *31*, 372−378.
(8) Xiong, J.; Hu, S.; Liu, Y.; Yu, J.; Yu, H.; Xie, L.; Wen, J.; Wang, X. Polypropylene Modified with Amidoxime/Carboxyl Groups in Separating Uranium(VI) from Thorium(IV) in Aqueous Solutions. *ACS Sustainable Chem. Eng.* **2017**, *5*, 1924−1930.
(9) El-Magied, M. O. A.; Elshehy, E. A.; Manaa, E.-S. A.; Tolba, A. A.; Atia, A. A. Kinetics and Thermodynamics Studies on the Recovery of Thorium Ions Using Amino Resins with Magnetic Properties. *Ind. Eng. Chem. Res.* **2016**, *55*, 11338−11345.
(10) Anirudhan, T. S.; Rejeena, S. R. Thorium(IV) Removal and Recovery from Aqueous Solutions using Tannin-Modified Poly-(glycidylmethacrylate)-Grafted Zirconium oxide Densified Cellulose. *Ind. Eng. Chem. Res.* **2011**, *50*, 13288−13298.
(11) Anirudhan, T. S.; Suchithra, P. S.; Senan, P.; Tharun, A. R. Kinetic and Equilibrium Profiles of Adsorptive Recovery of Thorium-(IV) from Aqueous Solutions Using Poly(methacrylic acid) Grafted Cellulose/Bentonite Superabsorbent Composite. *Ind. Eng. Chem. Res.* **2012**, *51*, 4825−4836.
(12) Hosseini-Bandegharaei, A.; Allahabadi, A.; Rahmani-Sani, A.; Rastegar, A.; Khamirchi, R.; Mehrpouyan, M.; Hekmat-Shoar, R.; Pajohankia, Z. Thorium removal from weakly acidic solutions using titan yellow-impregnated XAD-7 resin beads: kinetics, equilibrium and thermodynamic studies. *J. Radioanal. Nucl. Chem.* **2016**, *309*, 761−776.
(13) Huang, Y.; Zheng, H.; Li, H.; Zhang, Z.; zhao, C.; Gou, Q.; Liu, Y. Highly effective and selective adsorption of thorium(IV) from aqueous solution using mesoporous graphite carbon nitride prepared by sol−gel template method. *Chem. Eng. J.* **2021**, *410*, 128321.
(14) Xiong, X. H.; Tao, Y.; Yu, Z. W.; Yang, L. X.; Sun, L. J.; Fan, Y. L.; Luo, F. Selective extraction of thorium from uranium and rare earth elements using sulfonated covalent organic framework and its membrane derivate. *Chem. Eng. J.* **2020**, *384*, 123240.
(15) Juère, E.; Florek, J.; Larivière, D.; Kim, K.; Kleitz, F. Support effects in rare earth element separation using diglycolamide-functionalized mesoporous silica. *New J. Chem.* **2016**, *40*, 4325−4334.
(16) Parsons-Moss, T.; Jones, S.; Wang, J.; Wu, Z.; Uribe, E.; Zhao, D.; Nitsche, H. Reduction of plutonium in acidic solutions by mesoporous carbons. *J. Radioanal. Nucl. Chem.* **2016**, *307*, 2593−2601.
(17) Perreault, L. L.; Giret, S.; Gagnon, M.; Florek, J.; Larivière, D.; Kleitz, F. Functionalization of Mesoporous Carbon Materials for Selective Separation of Lanthanides under Acidic Conditions. *ACS Appl. Mater. Interfaces* **2017**, *9*, 12003−12012.
(18) Wang, Z.; Brown, A. T.; Tan, K.; Chabal, Y. J.; Balkus, K. J., Jr. Selective Extraction of Thorium from Rare Earth Elements Using Wrinkled Mesoporous Carbon. *J. Am. Chem. Soc.* **2018**, *140*, 14735−14739.
(19) Xu, S.; Zhao, Y.; Zheng, F.; Zhang, Y. Hollow Fe3O4@ mesoporous carbon core−shell microspheres for efficient sorption of radionuclides. *J. Mater. Sci.* **2016**, *51*, 2550−2557.
(20) Yuan, L.-Y.; Liu, Y.-L.; Shi, W.-Q.; Lv, Y.-L.; Lan, J.-H.; Zhao, Y.-L.; Chai, Z.-F. High performance of phosphonate-functionalized mesoporous silica for U(vi) sorption from aqueous solution. *Dalton Trans.* **2011**, *40*, 7446−7453.
(21) Zhang, Z.-b.; Zhou, Y.-d.; Liu, Y.-H.; Cao, X.-h.; Zhou, Z.-w.; Han, B.; Liang, P.; Xiong, G.-x. Removal of thorium from aqueous solution by ordered mesoporous carbon CMK-3. *J. Radioanal. Nucl. Chem.* **2014**, *302*, 9−16.
(22) Kaygun, A. K.; Akyil, S. Study of the behaviour of thorium adsorption on PAN/zeolite composite adsorbent. *J. Hazard. Mater.* **2007**, *147*, 357−62.
(23) Sravani, V. V.; Sengupta, S.; Sreenivasulu, B.; Gopakumar, G.; Tripathi, S.; Chandra, M.; Rao, C. V. S. B.; Suresh, A.; Nagarajan, S. Highly efficient functionalized MOF-LIC-1 for extraction of U(vi) and Th(iv) from aqueous solution: experimental and theoretical studies. *Dalton Trans.* **2022**, *51*, 3557−3571.
(24) Abdelhamid, H. N. Solid Acid Zirconium Oxo Sulfate/Carbon-Derived UiO-66 for Hydrogen Production. *Energy Fuels* **2021**, *35*, 10322−10326.
(25) Gumber, N.; Pai, R. V.; Sanyal, K.; Dutta, B.; Hassan, P. A. Synthesis and uranium adsorption studies of UiO-66 (Ce) based metal organic frameworks from aqueous solutions. *Microporous Mesoporous Mater.* **2022**, *341*, 112108.
(26) Espallargas, G. M.; Coronado, E. Magnetic functionalities in MOFs: from the framework to the pore. *Chem. Soc. Rev.* **2018**, *47*, 533−557.
(27) Sun, Y.; Zheng, L.; Yang, Y.; Qian, X.; Fu, T.; Li, X.; Yang, Z.; Yan, H.; Cui, C.; Tan, W. Metal−Organic Framework Nanocarriers for Drug Delivery in Biomedical Applications. *Nano-Micro Lett.* **2020**, *12*, 103.
(28) Falaise, C.; Volkringer, C.; Giovine, R.; Prelot, B.; Huve, M.; Loiseau, T. Capture of actinides (Th4+, [UO2]2+) and surrogating lanthanide (Nd3+) in porous metal−organic framework MIL-100(Al) from water: selectivity and imaging of embedded nanoparticles. *Dalton Trans.* **2017**, *46*, 12010−12014.
(29) Guo, X.-G.; Qiu, S.; Chen, X.; Gong, Y.; Sun, X. Postsynthesis Modification of a Metallosalen-Containing Metal−Organic Framework for Selective Th(IV)/Ln(III) Separation. *Inorg. Chem.* **2017**, *56*, 12357−12361.
(30) Liu, W.; Dai, X.; Wang, Y.; Song, L.; Zhang, L.; Zhang, D.; Xie, J.; Chen, L.; Diwu, J.; Wang, J.; Chai, Z.; Wang, S. Ratiometric Monitoring of Thorium Contamination in Natural Water Using a Dual-Emission Luminescent Europium Organic Framework. *Environ. Sci. Technol.* **2019**, *53*, 332−341.

https://doi.org/10.1021/acsomega.2c08274
ACS Omega 2023, 8, 12268−12282

(31) Xiong, Y.; Gao, Y.; Guo, X.; Wang, Y.; Su, X.; Sun, X. Water-Stable Metal−Organic Framework Material with Uncoordinated Terpyridine Site for Selective Th(IV)/Ln(III) Separation. *ACS Sustainable Chem. Eng.* **2019**, *7*, 3120−3126.
(32) Zhang, N.; Yuan, L.-Y.; Guo, W.-L.; Luo, S.-Z.; Chai, Z.-F.; Shi, W.-Q. Extending the Use of Highly Porous and Functionalized MOFs to Th(IV) Capture. *ACS Appl. Mater. Interfaces* **2017**, *9*, 25216−25224.
(33) Howarth, A. J.; Liu, Y.; Li, P.; Li, Z.; Wang, T. C.; Hupp, J. T.; Farha, O. K. Chemical, thermal and mechanical stabilities of metal−organic frameworks. *Nat. Rev. Mater.* **2016**, *1*, 15018.
(34) Doty, F. P.; Bauer, C. A.; Grant, P. G.; Simmons, B. A.; Skulan, A. J.; Allendorf, M. D. Radioluminescence and radiation effects in metal organic framework materials. *Penetrating Radiation Systems and Applications VIII*; SPIE, 2007; p 67070F.
(35) Hanna, S. L.; Rademacher, D. X.; Hanson, D. J.; Islamoglu, T.; Olszewski, A. K.; Nenoff, T. M.; Farha, O. K. Structural Features of Zirconium-Based Metal−Organic Frameworks Affecting Radiolytic Stability. *Ind. Eng. Chem. Res.* **2020**, *59*, 7520−7526.
(36) Volkringer, C.; Falaise, C.; Devaux, P.; Giovine, R.; Stevenson, V.; Pourpoint, F.; Lafon, O.; Osmond, M.; Jeanjacques, C.; Marcillaud, B.; Sabroux, J. C.; Loiseau, T. Stability of metal−organic frameworks under gamma irradiation. *Chem. Commun.* **2016**, *52*, 12502−12505.
(37) Li, Z.-J.; Ju, Y.; Lu, H.; Wu, X.; Yu, X.; Li, Y.; Wu, X.; Zhang, Z.-H.; Lin, J.; Qian, Y.; He, M.-Y.; Wang, J.-Q. Boosting the Iodine Adsorption and Radioresistance of Th-UiO-66 MOFs via Aromatic Substitution. *Chem.—Eur. J.* **2021**, *27*, 1286−1291.
(38) Ma, C.; Liu, H.; Wolterbeek, H. T.; Denkova, A. G.; Serra Crespo, P. Effects of High Gamma Doses on the Structural Stability of Metal−Organic Frameworks. *Langmuir* **2022**, *38*, 8928−8933.
(39) Qian, X.; Zhang, R.; Chen, L.; Lei, Y.; Xu, A. Surface Hydrophobic Treatment of Water-Sensitive DUT-4 Metal−Organic Framework To Enhance Water Stability for Hydrogen Storage. *ACS Sustainable Chem. Eng.* **2019**, *7*, 16007−16012.
(40) Álvarez, J. R.; Sánchez-González, E.; Pérez, E.; Schneider-Revueltas, E.; Martínez, A.; Tejeda-Cruz, A.; Islas-Jácome, A.; González-Zamora, E.; Ibarra, I. A. Structure stability of HKUST-1 towards water and ethanol and their effect on its CO2 capture properties. *Dalton Trans.* **2017**, *46*, 9192−9200.
(41) Olsen, J. V.; Kirkegaard, P.; Pedersen, N. J.; Eldrup, M. PALSfit: A new program for the evaluation of positron lifetime spectra. *Phys. Status Solidi C* **2007**, *4*, 4004−4006.
(42) Ahnfeldt, T.; Guillou, N.; Gunzelmann, D.; Margiolaki, I.; Loiseau, T.; Férey, G.; Senker, J.; Stock, N. [Al4(OH)2(OCH3)4-(H2N-bdc)3]·x H2O: A 12-Connected Porous Metal−Organic Framework with an Unprecedented Aluminum-Containing Brick. *Angew. Chem., Int. Ed.* **2009**, *48*, 5163−5166.
(43) Si, X.; Jiao, C.; Li, F.; Zhang, J.; Wang, S.; Liu, S.; Li, Z.; Sun, L.; Xu, F.; Gabelica, Z.; Schick, C. High and selective CO2 uptake, H2storage and methanol sensing on the amine-rdecorated 12-connected MOF CAU-1. *Energy Environ. Sci.* **2011**, *4*, 4522−4527.
(44) Horváth, G.; Kawazoe, K.; Th, G.; Kawazoe, K. Method For The Calculation Of Effective Pore Size Distribution In Molecular Sieve Carbon. *J. Chem. Eng. Jpn.* **1983**, *16*, 470−475.
(45) Jean, Y. C. Positron annihilation spectroscopy for chemical analysis: A novel probe for microstructural analysis of polymers. *Microchem. J.* **1990**, *42*, 72−102.
(46) Eldrup, M.; Lightbody, D.; Sherwood, J. N. The temperature dependence of positron lifetimes in solid pivalic acid. *Chem. Phys.* **1981**, *63*, 51−58.
(47) Tao, S. J. Positronium Annihilation in Molecular Substances. *J. Chem. Phys.* **1972**, *56*, 5499−5510.
(48) Warringham, R.; Gerchow, L.; Cooke, D.; Crivelli, P.; Vallery, R. S.; Mitchell, S.; Pérez-Ramírez, J. Acidity Effects in Positron Annihilation Lifetime Spectroscopy of Zeolites. *J. Phys. Chem. C* **2018**, *122*, 3443−3453.
(49) Atta, A. M.; Akl, Z. F. Removal of thorium from water using modified magnetite nanoparticles capped with rosin amidoxime. *Mater. Chem. Phys.* **2015**, *163*, 253−261.
(50) Lin, C.; Wang, H.; Wang, Y.; Cheng, Z. Selective solid-phase extraction of trace thorium(IV) using surface-grafted Th(IV)-imprinted polymers with pyrazole derivative. *Talanta* **2010**, *81*, 30−6.
(51) Humelnicu, D.; Drochioiu, G.; Sturza, M. I.; Cecal, A.; Popa, K. Kinetic and thermodynamic aspects of U(VI) and Th(IV) sorption on a zeolitic volcanic tuff. *J. Radioanal. Nucl. Chem.* **2006**, *270*, 637−640.
(52) Kaynar, Ü. H.; Ayvacıklı, M.; Hiçsönmez, Ü.; Çam Kaynar, S. Removal of thorium (IV) ions from aqueous solution by a novel nanoporous ZnO: Isotherms, kinetic and thermodynamic studies. *J. Environ. Radioact.* **2015**, *150*, 145−151.
(53) Nilchi, A.; Dehaghan, T. S.; Garmarodi, S. R. Kinetics, isotherm and thermodynamics for uranium and thorium ions adsorption from aqueous solutions by crystalline tin oxide nanoparticles. *Desalination* **2013**, *321*, 67−71.
(54) Teksöz, S.; Acar, Ç.; Ünak, P. Hydrolytic Behavior of Th4+, UO22+, and Ce3+ Ions at Various Temperatures. *J. Chem. Eng. Data* **2009**, *54*, 1183−1188.
(55) Gode, F.; Pehlivan, E. A comparative study of two chelating ion-exchange resins for the removal of chromium(III) from aqueous solution. *J. Hazard. Mater.* **2003**, *100*, 231−43.
(56) Gode, F.; Pehlivan, E. Adsorption of Cr(III) ions by Turkish brown coals. *Fuel Process. Technol.* **2005**, *86*, 875−884.
(57) Ho, Y.-S. Effect of pH on lead removal from water using tree fern as the sorbent. *Bioresour. Technol.* **2005**, *96*, 1292−1296.
(58) Hameed, B. H.; Chin, L. H.; Rengaraj, S. Adsorption of 4-chlorophenol onto activated carbon prepared from rattan sawdust. *Desalination* **2008**, *225*, 185−198.
(59) Hu, K.; Liu, Z.; Xiu, T.; Zhou, L.; Wang, Y. Removal of thorium from aqueous solution by adsorption with Cu3(BTC)2. *J. Radioanal. Nucl. Chem.* **2020**, *326*, 185−192.
(60) Moghaddam, Z. S.; Kaykhaii, M.; Khajeh, M.; Oveisi, A. R. Synthesis of UiO-66-OH zirconium metal-organic framework and its application for selective extraction and trace determination of thorium in water samples by spectrophotometry. *Spectrochim. Acta, Part A* **2018**, *194*, 76−82.
(61) Khouya, E. H.; Legrouri, K.; Fakhi, S.; Hannache, H. Adsorption of uranium and thorium on new adsorbent prepared from Moroccan oil shale impregnated with phosphoric acid. *Nat. Precedings* **2010**, 1.
(62) Gado, M. A.; Atia, B. M.; Cheira, M. F.; Abdou, A. A. Thorium ions adsorption from aqueous solution by amino naphthol sulphonate coupled chitosan. *Int. J. Environ. Anal. Chem.* **2021**, *101*, 1419−1436.
(63) Kaynar, U. H.; Şabikoğlu, İ. Adsorption of thorium (IV) by amorphous silica; response surface modelling and optimization. *J. Radioanal. Nucl. Chem.* **2018**, *318*, 823−834.
(64) Salah, A.; Gaber, S.; Kandil, T. The Removal of Uranium and Thorium from Their Aqueous Solutions by 8-Hydroxyquinoline Immobilized Bentonite. *Minerals* **2019**, *9*, 626.
(65) Pearson, R. G. Hard and soft acids and bases, HSAB, part 1: Fundamental principles. *J. Chem. Educ.* **1968**, *45*, 581.
(66) Hemmingsen, L.; Amara, P.; Ansoborlo, E.; Field, M. J. Importance of Charge Transfer and Polarization Effects for the Modeling of Uranyl−Cation Complexes. *J. Phys. Chem. A* **2000**, *104*, 4095−4101.
(67) Pagnanelli, F.; Papini, M. P.; L.Toro, M.; Trifoni, F.; Vegliò, F. Biosorption of Metal Ions on Arthrobacter sp.: Biomass Characterization and Biosorption Modeling. *Environ. Sci. Technol.* **2000**, *34*, 2773−2778.
(68) Kazy, S. K.; D'Souza, S. F.; Sar, P. Uranium and thorium sequestration by a Pseudomonas sp.: Mechanism and chemical characterization. *J. Hazard. Mater.* **2009**, *163*, 65−72.
(69) Ding, M.; Chen, L.; Xu, Y.; Chen, B.; Ding, J.; Wu, R.; Huang, C.; He, Y.; Jin, Y.; Xia, C. Efficient capture of Tc/Re(VII, IV) by a viologen-based organic polymer containing tetraaza macrocycles. *Chem. Eng. J.* **2020**, *380*, 122581.

https://doi.org/10.1021/acsomega.2c08274
ACS Omega 2023, 8, 12268−12282

(70) Moulder, J. F.; Chastain, J. *Handbook of X-ray Photoelectron Spectroscopy: A Reference Book of Standard Spectra for Identification and Interpretation of XPS Data*; Physical Electronics Division, Perkin-Elmer Corporation, 1992.
(71) Aziman, E. S.; Salehuddin, A. H. J. M.; Ismail, A. F. Remediation of Thorium (IV) from Wastewater: Current Status and Way Forward. *Separ. Purif. Rev.* **2021**, *50*, 177−202.
(72) Yang, T.; Tsushima, S.; Suzuki, A. Quantum Mechanical and Molecular Dynamical Simulations on Thorium(IV) Hydrates in Aqueous Solution. *J. Phys. Chem. A* **2001**, *105*, 10439−10445.
(73) Šulka, M.; Cantrel, L.; Vallet, V. Theoretical Study of Plutonium(IV) Complexes Formed within the PUREX Process: A Proposal of a Plutonium Surrogate in Fire Conditions. *J. Phys. Chem. A* **2014**, *118*, 10073−10080.

https://doi.org/10.1021/acsomega.2c08274
ACS Omega 2023, 8, 12268−12282